# FIRST 2.2 $\mu$m RESULTS FROM THE IOTA INTERFEROMETER

H. M. DYCK

Department of Physics & Astronomy, University of Wyoming, Laramie, Wyoming 82071
Electronic mail: meldyck@uwyo.edu

J. A. BENSON, N. P. CARLETON, C. COLDWELL, M. G. LACASSE, P. NISENSON, A. PANASYUK, C. PAPALIOLIOS, M. R. PEARLMAN, R. D. REASENBERG, W. A. TRAUB, AND X. XU

Harvard/Smithsonian Center for Astrophysics, Cambridge, Massachusetts 02138
Electronic mail: benson@noao.edu, carleton@cfa.harvard.edu, coldwell@iotavax.sao.arizona.edu, lacasse@cfa.harvard.edu, nisenson@cfa.harvard.edu, panasyuk@cfa.harvard.edu, papaliolios@huhepl.harvard.edu, pearlman@cfa.harvard.edu, reasenberg@cfa.harvard.edu, traub@cfa.harvard.edu, xu@cfa.harvard.edu

C. R. PREDMORE AND F. P. SCHLOERB

Department of Physics and Astronomy, University of Massachusetts, Amherst, Massachusetts 01003
Electronic mail: predmore@fcrao1.phast.umass.edu, schloerb@fcrao1.phast.umass.edu

D. M. GIBSON

MIT Lincoln Laboratory, Socorro, New Mexico 87801
Electronic mail: gibson@ll.mit.edu

*Received 1994 July 21; revised 1994 August 18*

## ABSTRACT

We present the first infrared fringe visibility measurements made with the Infrared Optical Telescope Array on Mt. Hopkins. Effective temperatures are derived for RX Boo, RS Cnc, and $\beta$ Peg. RX Boo is the coolest small-amplitude variable giant star to have an effective temperature determination. We compare the size of its photosphere at infrared wavelengths with the sizes of its SiO and $H_2O$ radio emission regions. We also discuss initial performance parameters for the interferometer.

## 1. INTRODUCTION

The application of Michelson stellar interferometers to the measurement of fundamental stellar parameters at optical and infrared wavelengths is a well established technology. Angular diameters for more than 50 stars have been reported, some with precisions better than 1% (DiBenedetto & Rabbia 1987; Dyck *et al.* 1993; Mozurkewich *et al.* 1991). Interferometers are also capable of yielding orbits for spectroscopic binaries (Armstrong *et al.* 1992) and information about the structure of circumstellar shells (Bester *et al.* 1991). Direct measurements of limb darkening and surface structure now seem possible. The Infrared Optical Telescope Array (IOTA) is a new three-telescope Michelson interferometer array designed to address these problems and to explore phase-closure imaging. Situated near the summit of Mt. Hopkins in Southern Arizona, IOTA now has two telescopes in place and obtained its first infrared fringes in December 1993 (Carleton *et al.* 1994). Although the interferometer is currently in its final construction and testing phases and the optical alignment and operating procedures are still under development, it has been used to begin some scientific projects at near infrared wavelengths.

In this paper we report new observations of two very cool red giants—RS Cnc and RX Boo. RS Cnc is a high-luminosity star classified M6 Ib–II with mild S characteristics (Keenan 1954; Sharpless 1956). RX Boo is classified as a giant of spectral type M7.5–M8 (Keenan & McNeil 1989). Both stars show evidence for circumstellar dust and gas shells; Knapp & Morris (1985) estimate modest mass loss rates of order 3–4 $10^{-7}$ $\mathscr{M}_\odot$/yr from analysis of the CO emission. RX Boo has maser emission from $H_2O$ (Bowers *et al.* 1993) and thermal emission from SiO (Sahai & Bieging 1993). Our angular diameter measurements allow us to compare the sizes of the radio emitting regions directly to the photosphere size. Observations of RX Boo extend the effective temperature sequence for small-amplitude variable giants to the coolest spectral type yet available. We also report one observation of $\beta$ Peg which has been measured previously at CERGA (DiBenedetto & Rabbia 1987).

## 2. OBSERVATIONS AND DATA REDUCTION

The goals and design strategies of IOTA have been reported elsewhere (cf. Carleton *et al.* 1994; Reasenberg 1990) and will not be repeated here. Parallel light beams from the two telescopes are combined onto a beam splitter and then focused onto a pair of InSb photovoltaic detectors. For the work reported here, we used a $K$ filter (2.2 $\mu$m, 18% spectral bandwidth) and a north–south baseline of 21.2 m. Fast autoguiding is employed to correct for atmospheric wavefront tilt errors and a high-precision, active, optical delay line is used to compensate for the earth's rotation. Only a limited range of optical delay line compensation was available at the time of the work, so we were limited to observations close to the zenith.

At IOTA we employ a data collection scheme which samples the entire fringe packet from the source. It is a slight

 0004-6256/95/109(1)/378/5/$0.90  

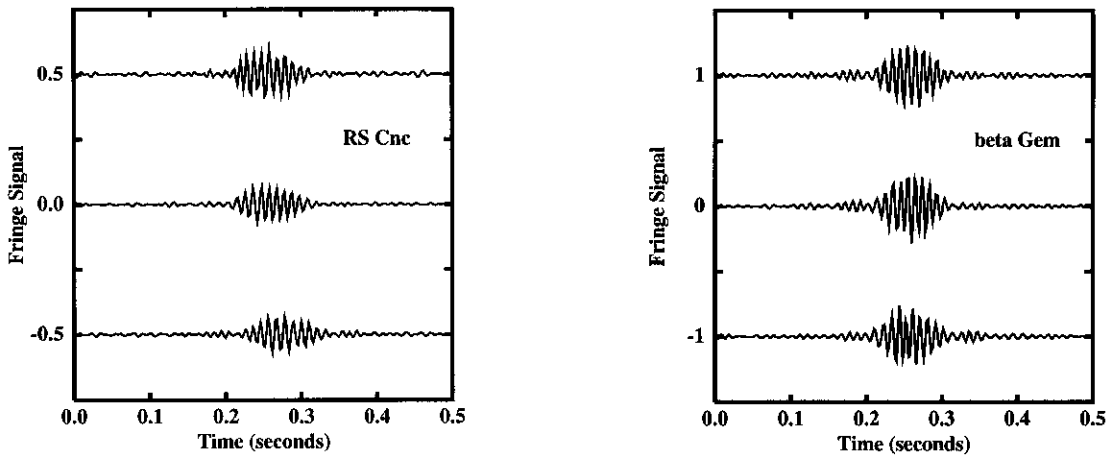


FIG. 1. A series of sequential interferograms for two stars: RS Cnc is a program star and $\beta$ Gem is a calibrator. The nominal fringe frequency is 100 Hz. The measured signals have been filtered in the Fourier domain by a 50–150 Hz bandpass filter, and offset on the vertical axis for clarity. Note the factor of two change in the vertical scale.

modification of the earth-rotation scanning procedure developed at CERGA (Gay & Mekarnia 1988) and also used at IRMA (Benson *et al.* 1991). With earth-rotation scanning, the zero-path position of the interferometer sweeps across the detector field of view producing a sinusoidal signal in the detectors. In the IOTA modification, the tracking delay line is propelled, under computer control, at a velocity which generates the fringe signal at a fixed frequency chosen to lie above most of the atmospheric noise. For observations reported here this nominal frequency was 100 Hz for all but one night when we used a frequency of 200 Hz.

For the work reported here, we point the interferometer at the source and search a 90 s time window for the fringe packet. When the equal path position for the interferometer is identified, we take a series of repeated scans on the source, each lasting 8 s, where the delay line is driven in one direction at the desired rate (the data collection part of the cycle) and in the other direction at a slew rate (the return part of the cycle). Thus, at present we expend 8 s of observing to obtain about 0.1 s of fringe data (the approximate duration of the fringe packet). As the interferometer becomes better characterized, the observation window will be decreased and the duty cycle will improve.

Signals from the two channels, $S_0$ and $S_1$, were corrected for dc offset. We then computed a raw fringe signal $F_{\mathrm{RAW}}=(S/\langle S\rangle)-1$ for each channel, where $\langle S\rangle$ is the mean signal level in the channel. These raw signals were Fourier transformed and filtered with a square filter of 100 Hz bandwidth centered on the fringe frequency. This filter is not the optimum one for our data but it allows for automatic data processing in the presence of the approximately $\pm 20\%$ variation which occurred in the fringe frequency. After filtering, the data were inverse transformed and the amplitude of the fringe pattern, $V'$ (the measured visibility), was determined for both channels by measuring the amplitudes of the four largest peaks near the center of the fringe packet. The nightly mean values of $V'$, and standard errors of the means, were computed for each star observed.

We tried two other data reduction schemes. In one, the fringe signal power spectrum was computed and the noise background subtracted. The square roots of these differences were accumulated for the nightly mean. The area under this square root distribution is proportional to the object visibility amplitude (Benson *et al.* 1994). In the other, an ideal fringe signal template was fitted to the filtered data, where the amplitude was one of the model parameters (cf. Carleton *et al.* 1994). One might expect that fitting all the fringes would yield a higher signal-to-noise ratio (S/N) estimate of the visibility amplitude than simply measuring four peaks. However, at this stage, the night-to-night variations have been found to be much greater than the internal dispersion. Thus, little practical difference was found among the three methods.

The instrumental visibilities were transformed into calibrated visibilities by using observations of standard stars for which the diameters were assumed to be known. These calibration sources and their adopted angular diameters, $\theta_{\mathrm{UD}}$, (computed assuming they are uniformly bright, circular disks) are given in Table 1. An ideal visibility was calculated for each of these standard stars. The uniform-disk visibility divided by the measured visibility for each calibration star yields an estimate of the instrumental response factor, $\gamma$. The inverse of these mean response factors (i.e., the point source

TABLE 1. Assumed diameters for calibration sources.

| Star | $\theta_{\mathrm{UD}}$ (mas) | Source for the Diameter |
|---|---|---|
| $\iota$ Aur | 7.0 | Black body determination |
| $\delta$ Boo | 2.8 | Blackwell & Lynas-Gray (1994) |
| $\varepsilon$ Boo | 5.1 | Black body determination |
| $\gamma$ Com | 3.1 | Black body determination |
| 41 Cyg | 1.0 | Blackwell *et al.* (1990) |
| $\beta$ Gem | 7.7 | DiBenedetto & Rabbia (1987) |
| $\alpha$ Lyn | 7.7 | DiBenedetto & Rabbia (1987) |
| $\psi$ Peg | 6.4 | Black body determination |
| $\beta$ Tau | 1.0 | Mozurkewich *et al.* (1991) |

TABLE 2. Calibrated visibilities in the two data channels.

| Date | Star | $B_P$(m) | $N$ | $V_0 \pm \varepsilon$ | $V_1 \pm \varepsilon$ |
|---|---|---|---|---|---|
| 1993 Dec 10 | RS Cnc | 21.2 | 17 | 0.55±0.04 | 0.58±0.04 |
| | $\beta$ Peg | 21.2 | 9 | 0.48±0.08 | 0.49±0.08 |
| 1994 Jan 14 | RS Cnc | 21.2 | 21 | 0.44±0.04 | 0.51±0.03 |
| 1994 Jan 20 | RS Cnc | 21.2 | 15 | 0.53±0.06 | 0.40±0.05 |
| 1994 Jan 21 | RX Boo | 21.1 | 25 | 0.24±0.04 | 0.26±0.03 |
| | RS Cnc | 21.2 | 20 | 0.42±0.04 | 0.42±0.04 |
| 1994 Apr 19 | RX Boo | 21.2 | 37 | 0.44±0.02 | 0.38±0.03 |
| 1994 May 05 | RX Boo | 21.2 | 21 | 0.51±0.04 | 0.47±0.04 |

response) averaged 0.22 between 1993 December and 1994 May. In order to minimize the effect of fluctuations in the instrumental response caused by variations in the atmospheric seeing and interferometer alignment, we tried to observe calibration stars close in time to the program stars. The raw program star visibilities were multiplied by the $\gamma$ obtained from the nearest calibrator to yield the calibrated visibilities, $V$. We have listed the mean calibrated visibilities for each channel, $\pm 1$ standard deviation of the mean (reflecting the observational scatter and the uncertainty in the calibration), the median projected baseline, and the number of observations in Table 2.

## 3. INITIAL PERFORMANCE EVALUATION

We have investigated the distribution of visibility amplitude measurements during the observation period. These are shown in Fig. 2, where we have plotted the value of the observed visibility divided by the mean visibility for each separate set of measurements. A Gaussian curve has been drawn through the data and is a reasonable approximation to the distribution. To first order, one might expect a roughly Gaussian distribution for the measured values, owing to the assumed random variation of atmospherically induced wavefront tilt and curvature. The average level, of course, will depend upon the quality of the optical elements and the alignment. The symmetry of the data in Fig. 2 suggests to us that the degree of misalignment of the interferometer is sufficiently great that the probabilities of the visibility being increased or decreased by random atmospheric perturbations are about equal. If the interferometer were perfectly aligned, then the distribution would be skewed toward lower values by all atmospheric perturbations. Of course, any other effect which degrades the visibility significantly can produce the same result. These effects might include poor seeing, vibrations in the instrument or incomplete correction for image wander by the star tracker.

There is evidence that the internal precision during a particular night is better than the night-to-night variation in visibilities. From limited repeated observations on the program

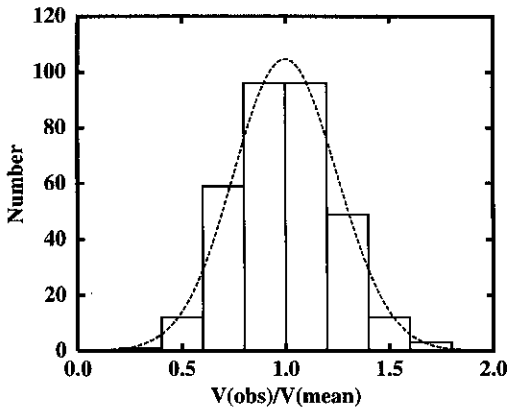


FIG. 2. The distribution of measured visibilities, normalized by the mean visibility, for observations reported here. The dashed curve is a Gaussian.

stars we judge that the rms night-to-night scatter is roughly $\pm 0.08$ in the visibility amplitude; the scatter on a particular night is about half that value. The larger variations probably arise from changes in the optical alignment of the interferometer from one night to the next, and incomplete compensation for these differences by observations of calibration standards. At present, we do not have sufficient data to characterize the distribution of these variations. We caution against strict interpretation of the night to night dispersion in terms of Gaussian statistics until we can demonstrate that this is, in fact, the case.

We may make some preliminary estimates of the sensitivity limit. The faintest star we have observed with readily apparent fringes has a brightness of $K=3.8$ and S/N=4.4 for a single scan. (Here, S/N refers to the ratio of the peak-to-peak fringe amplitude to the peak-to-peak noise in the filtered interferogram.) We can clearly recognize a fringe pattern in the surrounding noise when S/N=2. Therefore, we expect to recognize fringes instantaneously to a limit of $K=4.7$ in one interferogram. Even with no improvements to the interferometer it will clearly be possible to observe the brightest sources in nearby giant molecular clouds, such as the BN source, as well as the brightest T Tauri and Be/Ae stars.

## 4. RESULTS AND DISCUSSION

Average calibrated visibilities, weighted by the inverse square of the standard deviations, were computed for the three program stars, RX Boo, RS Cnc, and $\beta$ Peg and are listed in Table 3. The errors were computed from the night-to-night dispersion and have not been weighted. For the visibility error for $\beta$ Peg, where we have only one observation,

TABLE 3. Derived angular diameters and effective temperatures.

| Star | $V \pm \varepsilon$ | $\theta_{UD}$ (mas) | $\theta_{LD}$ (mas) | $\theta_R$ (mas) | $F_{TOT}$ (W cm$^{-2}$ | $T_{EFF}$ (K) |
|---|---|---|---|---|---|---|
| RX Boo | 0.39±0.05 | 17.2±0.9 | 18.7±1.0 | 17.6±0.9 | $8.43\times10^{-13}$ | 3015±105 |
| RS Cnc | 0.48±0.02 | 15.5±0.4 | 17.2±0.4 | 15.8±0.4 | $7.47\times10^{-13}$ | 3085±110 |
| $\beta$ Peg | 0.49±0.06 | 15.3±1.1 | 16.4±1.2 | 15.6±1.1 | $1.57\times10^{-12}$ | 3740±130 |

we have adopted $\pm 0.08$ following our discussion above. The weighted mean visibilities were used to derive a uniform-disk angular diameter, $\theta_{UD}$, in milliarcsec (mas), for each star; these are also listed in Table 3.

In order to compute effective temperatures, $T_{EFF}$, we need to convert the uniform disk angular diameters to appropriate limb-darkened angular diameters. We adopt the convention suggested by Scholz (1985), where a fictitious stellar radius corresponding to the Rosseland mean opacity at $\tau_R = 1$ is chosen as the appropriate surface to represent the effective temperature. We have used the center-to-limb brightness profiles computed by Scholz & Takeda (1987) using extended spherical atmospheres and opacities relevant to the low temperatures considered here. From the model profiles, we have computed a scaling factor to convert the uniform-disk diameter to a limb-darkened diameter, $\theta_{LD}$, at a particular wavelength. Their model calculations for 2.17 $\mu$m correspond most closely to the effective wavelength of our observations. The scaling factors increase the uniform-disk diameters by amounts ranging from about 7% for a giant star with $T_{EFF} = 3500$ K (model U3500) to about 11% for a supergiant with $T_{EFF} = 3000$ K (model X3000). For each model, we have then rescaled the angular diameter to the Rosseland mean angular diameter, $\theta_R$, using information provided with each of the brightness profiles. The result of this operation is that the limb-darkened diameters are decreased such that $\theta_R \approx 1.022\theta_{UD}$, **independent of model $T_{EFF}$ and luminosity.** We have used this factor to convert the uniform-disk diameters to Rosseland mean diameters. Both $\theta_{LD}$ and $\theta_R$ have been listed in Table 3. Using $\theta_R$ to compute the effective temperature has the advantage of yielding approximately the same factor that DiBenedetto & Rabbia (1987) used to convert uniform-disk diameters to limb-darkened diameters, based upon plane-parallel atmospheres (Manduca 1979). Thus, a direct comparison of effective temperatures obtained with the CERGA interferometer and with IOTA may be made.

The effective temperature for a star may be computed from

$$T_{EFF} = 1.32 \times 10^7 \left( \frac{F_{TOT}}{\theta_R^2} \right)^{1/4},$$

where $F_{TOT}$ is the total flux density from the star, in W cm$^{-2}$, and $\theta_R$ is in units of mas. We have obtained the total fluxes for the three stars in Table 2 from various sources in the literature, including Gezari *et al.* (1993), Lee (1970), Lockwood (1972), and Neugebauer *et al.* (1986) for RX Boo and RS Cnc, and from Blackwell *et al.* (1990) for $\beta$ Peg. The adopted values of $F_{TOT}$ and the corresponding $T_{EFF}$ have also been listed in Table 3. The errors in $T_{EFF}$ arise from three sources—errors in the measured diameter, errors in the flux calibration, and unknown levels of brightness variation in the program stars. We have estimated the flux calibration to be accurate to $\pm 5\%$ (see the recent discussion of this problem in Blackwell & Lynas-Gray 1994). From an inspection of the tabulated data in Gezari *et al.* (1993), we believe that the total flux variation for RX Boo and RS Cnc will be of order $\pm 10\%$, or less. We believe that $\pm 10\%$ is a reasonable estimate of the error from this source. The final error is dominated by the flux errors; therefore, we have adopted identical estimated errors in $T_{EFF}$ of $\pm 3.5\%$ for these two stars.

For $\beta$ Peg, the most significant source of error undoubtedly arises from the fact that we have only one measurement. By adopting a conservative estimate for the visibility error we obtain a uniform disk diameter with a relatively large error. Nevertheless, it is of interest to compare our value, $\theta_{UD} = 15.3 \pm 1.1$ mas, to the $\theta_{UD} = 16.2 \pm 0.2$ mas obtained by DiBenedetto & Rabbia (1987). Our value is 0.9 mas smaller than theirs, although it is within our estimated uncertainty. Quirrenbach *et al.* (1993) have compared their estimates of limb-darkened diameters for various red giants with those reported by DiBenedetto & Rabbia and have concluded that there may be a slight systematic difference, possibly attributable to an uncompensated bias in the CERGA data. The sense of the difference is that the CERGA observations appear to produce a smaller limb-darkened diameter than do the Mark III measurements. Quirrenbach *et al.* estimate $\theta_{LD} = 17.24$ mas at $\lambda = 0.754$ $\mu$m for $\beta$ Peg while DiBenedetto & Rabbia estimate $\theta_{LD} = 16.75 \pm 0.24$ mas at 2.2 $\mu$m; our value at 2.2 $\mu$m is $\theta_{LD} = 16.4 \pm 1.2$ mas. Although it is premature to use our datum to settle this question, owing to the large error, our diameter agrees better with the DiBenedetto & Rabbia estimate than with the one by Quirrenbach *et al.* The error associated with flux variations is probably smaller than the errors from other sources; we have also adopted an error of $\pm 3.5\%$ for $T_{EFF}$.

Our derived temperature for RX Boo is in agreement with an extrapolation of the calibration by Ridgway *et al.* (1980). At M7.5–M8, this star is the coolest small-amplitude variable giant star for which an effective temperature determination has been made. For RS Cnc, our effective temperature is about 165 K cooler than the corresponding luminosity class III temperatures in the Ridgway *et al.* calibration. This result is consistent with the temperature determinations for $\alpha$ Her and $\alpha$ Ori made with IRMA (Benson *et al.* 1991; Dyck *et al.* 1992) which were found to be cooler than the lower luminosity temperatures at the same spectral type.

RX Boo is interesting because of its extensive circumstellar gas and dust shell. We may compare our angular diameter to sizes determined by other techniques. For this, we use the estimate of the limb-darkened diameter, $\theta_{LD} \approx 19$ mas, reasoning that this diameter is a closer measure of the actual physical extension of the star at this wavelength than is the Rosseland mean angular diameter. Bowers *et al.* (1993) have mapped the distribution of $H_2O$ masers and found the masing region to have a diameter of about 150 mas. This is about 8 times the size of the 2.2 $\mu$m photosphere. Dyck & Benson (1992) have partially resolved the dust shell using speckle interferometry techniques at 10 $\mu$m. Their measurements indicate that the shell must be larger than about 270 mas. If these speckle data may be interpreted as measuring the inner diameter of the dust distribution, then the data indicate that dust condenses at distances greater than about 14 $R_*$ in this star. It also demonstrates that the water maser region lies well inside this condensation radius. Young *et al.* (1993) judge the extent of the dust envelope to be of order 10 arcmin, from analysis of the *IRAS* data. The region producing the SiO thermal emission has been measured by Sahai &

Bieging (1993) to be roughly 2.7 arcsec. This is of order 140 times the near-infrared photospheric size. Having accurate estimates of these dimensions will help one understand how grains form and evolve as they move outward through the shell and their effect on other observable properties of the circumstellar environment.

We thank Nathan Hazen, Walter Allen, Paul Horowitz, Kay Carleton, Nils Turner, Christine Woods, Kathy Carels, and the staff at the F. L. Whipple Observatory for help with engineering and construction on the project and Steve Ridgeway for valuable scientific discussions. We have had partial financial support from a NASA Innovative Research Projects Grant (NSG-7176) to Harvard University and from an NSF Grant (AST-9021181) to the University of Wyoming. This research has made use of the Simbad database, operated by the CDS, Strasbourg, France.

## REFERENCES

Armstrong, J. T., *et al.* 1992, AJ, 104, 241
Benson, J. A., *et al.* 1991, AJ, 102, 2091
Benson, J. A., Dyck, H. M., & Howell, R. R. 1994, Applied Optics (in press)
Bester, M., *et al.* 1991, ApJ, 367, L27
Blackwell, D. E., *et al.* 1990, A&A, 232, 396
Blackwell, D. E., & Lynas-Gray, A. E. 1994, A&A, 282, 899
Bowers, P. F., Claussen, M. J., & Johnston, K. J. 1993, AJ, 105, 284
Carleton, N. P., *et al.* 1994, Proc. SPIE, 2200, 152
DiBenedetto, G. P., & Rabbia, Y. 1987, A&A, 188, 114
Dyck, H. M., & Benson, J. A. 1992, AJ, 104, 377
Dyck, H. M., Benson, J. A., Ridgway, S. T., & Dixon, D. J. 1992, AJ, 104, 1982
Dyck, H. M., Benson, J. A., & Ridgway, S. T. 1993, PASP, 105, 610
Gay, J., & Mekarnia, D. 1988, in High-Resolution Imaging by Interferometry, edited by F. Merkle (European Southern Observatory, Garching bei München), p. 811
Gezari, D. Y., Schmitz, M., Pitts, P. S., & Mead, J. M. 1993, Catalog of Infrared Observations, NASA Reference Publication 1294
Keenan, P. C. 1954, ApJ, 120, 484
Keenan, P. C., & McNeil, R. C. 1989, ApJS, 71, 245
Knapp, G. R., & Morris, M. 1985, ApJ, 292, 640
Lee, T. A. 1970, ApJ, 162, 217
Lockwood, G. W. 1972, ApJS, 24, 375
Manduca, A. 1979, A&AS, 36, 411
Mozurkewich, D., *et al.* 1991, AJ, 101, 2207
Neugebauer, G., *et al.* 1986, A&AS, 65, 607
Quirrenbach, A., *et al.* 1993, ApJ, 406, 215
Reasenberg, R. D. 1990, Proc. SPIE, 1237, 128
Ridgway, S. T., Joyce, R. R., White, N. M., & Wing, R. F. 1980, AJ, 235, 126
Sahai, R., & Bieging, J. H. 1993, AJ, 105, 595
Scholz, M. 1985, A&A, 145, 251
Scholz, M., & Takeda, Y. 1987, A&A, 186, 200
Sharpless, S. 1956, ApJ, 124, 342
Young, K., Phillips, T. G., & Knapp, G. R. 1993, ApJS, 86, 517